Kinetics of strain-induced transformation of dispersed austenite in low-alloy TRIP steels

G.N. Haidemenopoulos [a,*], N. Aravas [a,b], I. Bellas [a]

[a] Department of Mechanical Engineering, University of Thessaly, 38334 Volos, Greece
[b] International Institute for Carbon Neutral Energy Research (WPI-I2CNER), Kyushu University, 744 Moto-oka, Nishi-ku, Fukuoka 819-0395, Japan

ABSTRACT

A model describing the kinetics of the evolution of martensite volume fraction during the strain-induced transformation of dispersed austenite in low-alloy TRIP steels has been developed. The model is based on the modification of the nucleation site potency distribution by the applied stress and plastic strain for the description of the stress-assisted and strain-induced transformation regimes respectively. The model is fitted to available experimental data regarding the evolution of martensite as a function of plastic strain for several steels containing austenitic dispersions. Besides chemical composition of retained austenite and temperature, the model takes into account the effects of austenite particle size and stress triaxiality. Austenite particle size refinement has a strong stabilizing influence by retarding the strain-induced transformation kinetics. Stress triaxiality becomes important in stabilized austenite dispersions (either chemically stabilized or by size refinement) by enhancing the kinetics of the strain-induced transformation. The kinetic model can be used for the development of a constitutive model describing the mechanical behavior of TRIP steels.

© 2014 Elsevier B.V. All rights reserved.

1. Introduction

Low-alloy Transformation-Induced Plasticity (TRIP) steels possess a multiphase microstructure, which consists typically of ferrite, bainite and retained austenite. The retained austenite, with a typical volume fraction of 10–15%, is in the form of a particle dispersion. The high uniform elongation, and hence high formability, of these steels results from the strain-induced martensitic transformation of retained austenite. The control of the kinetics of the strain-induced transformation is the most important prerequisite in order to design compositions and processing routes for enhanced mechanical behavior in these steels. Chemical composition, austenite particle size, neighboring phases, and stress-triaxiality are the most important factors influencing the stability of retained austenite and the strain-induced transformation kinetics [1–6]. These factors are interrelated and it is difficult to separate each individual effect. In an effort to gain a deeper understanding on the effects of these factors, several models have been developed for the kinetics of strain-induced transformation of austenite in TRIP steels. These models have been reviewed by Samek et al. [7]. The model by Angel [8] and Ludwigson et al. [9] is empirical and takes into account autocatalytic effects, i.e., the acceleration of transformation by the transformation-induced generation of new martensitic nuclei. The model by Matsumura et al. [10], which was based on the work of Burke [11] and modified by Tsuchida et al. [12], takes into account the stability of austenite and autocatalytic effects. In the model proposed by Sugimoto et al. [13] the rate of transformation is proportional to the fraction of untransformed austenite and austenite stability. The model by Olson et al. [14] was the first to take into account the physical mechanisms of martensitic nucleation induced by plastic strain. In that model, shear band intersections were considered as the potential nucleation sites for the transformation. The rate of shear band formation is influenced by composition and temperature through the stacking fault energy. All models described above were developed for homogeneous austenitic alloys and do not take into account that, in low-alloy multiphase TRIP steels, the austenite phase is dispersed in the form of particles in the microstructure. Therefore, the effect of austenite particle size on transformation kinetics is not considered in the aforementioned models. Only recently Zhang et al. [15] investigated the effect of particle size through a modification of the Burke–Matsumura–Tsuchida model [10–12]; however, it was not possible to differentiate between the effects of particle size and carbon partitioning in the austenite. There are also experimental data showing that particle size and stress triaxiality have important influence on strain-induced transformation and associated mechanical behavior [16,17].

The aim of this work is to develop a kinetic model for the description of the fraction of martensite formed as a function of plastic strain in steels, where the austenite is present in the form

* Corresponding author. Tel.: +30 2421074062.
E-mail address: hgreg@mie.uth.gr (G.N. Haidemenopoulos).

of dispersed particles. The model is able to predict the effects of austenite particle size, chemical composition of austenite particles, temperature and stress-state triaxiality on the strain-induced transformation kinetics. In Section 2.1 a literature review of the basic elements of the martensite nucleation theory and the potency distribution of nucleation sites is presented. The new model is then described in Sections 2.2–2.4.

2. Model description

2.1. Martensitic nucleation and potency distribution of nucleation sites

The model is developed for a steel containing retained austenite in the form of dispersed particles of average volume v_p per particle (for the list of symbols refer to Table 1). Martensitic transformation can be mechanically-induced in these dispersed austenite particles by two distinct mechanisms: stress-assisted and strain-induced nucleation [18]. In the stress-assisted regime, martensite nucleates on pre-existing nucleation sites. Those are the same sites which operate during the traditional transformation on cooling. In the strain-induced regime, new and more potent nucleation sites are created by plastic deformation of the austenitic phase. As the steel is stressed and deformed plastically, retained austenite will transform to martensite by the simultaneous operation of both mechanisms. The stress-assisted mechanism prevails at stresses lower than the yield-strength of austenite, whereas the strain-induced mechanism prevails after the yield-strength has been surpassed. The volume fraction of martensite forming as a result of the mechanically-induced transformation is denoted by f. This is the relative volume fraction with respect to the initial volume fraction of austenite and has values between 0 and 1.

Table 1
List of symbols.

Symbol	Definition	Unit
n	Potency of nucleation site (number of crystal planes)	–
n^*	Critical value of n for martensitic nucleation	–
E_{str}	Elastic strain energy	J/mol
γ_s	Fault/matrix interfacial energy	J/m²
γ_f	Energy of martensitic embryo per unit area	J/m²
ρ	Density of atoms in the fault plane	mol/m²
ΔG_{ch}	Chemical driving force for martensitic transformation	J/mol
ΔG_σ	Mechanical contribution to driving force	J/mol
W_f	Frictional work of interface motion	J/mol
N_v^0	Number of nucleation sites of all potencies	m⁻³
N_v	Number of nucleation sites with sufficient potency to nucleate martensite (operational sites)	m⁻³
$N_v^{\sigma 0}$	Pre-existing nucleation sites	m⁻³
N_v^σ	Operational sites under applied stress σ	m⁻³
$N_v^{\varepsilon 0}$	Additional sites produced by plastic strain ε	m⁻³
N	Maximum number of sites that can be produced by plastic strain	m⁻³
N_v^ε	Operational nucleation sites at plastic strain ε	m⁻³
a	Shape factor of potency distribution	–
a_σ	Shape factor of stress-modified potency distribution	–
a_ε	Shape factor of strain-modified potency distribution	–
v_p	Average volume of austenite particles	m³
V^a	Austenite volume	m³
V^m	Martensite volume	m³
V	Total volume (austenite+martensite)	m⁻³
f	Volume fraction of mechanically-induced martensite	–
f_{SA}	Fraction of martensite by stress-assisted transformation	
α, m, k	Constants	–

The model is based on the Olson–Cohen theory of heterogeneous martensitic nucleation [19–21]. According to this theory, the formation of a martensitic nucleus takes place by the dissociation of an existing defect, which serves as a nucleation site for the transformation. Dissociation of such a defect creates a fault structure or martensitic embryo, the growth of which is determined by the energy change accompanying the dissociation. The energy per unit area of an embryo with a thickness of n crystal planes is denoted by $\gamma_f(n)$ and is given by

$$\gamma_f(n) = n\rho(\Delta G_{ch} + E_{str} + W_f) + 2\gamma_s, \tag{1}$$

where ΔG_{ch} is the chemical driving force for martensitic transformation (energy/mole), γ_s is the fault/matrix interfacial energy, ρ is the density of atoms in the fault plane (moles/unit area on a crystal plane), E_{str} is the elastic strain energy associated with distortions in the fault interface plane (energy/mole), and W_f is the frictional work of interfacial motion (energy/mole), which occurs during the dissociation process. Spontaneous martensitic nucleation occurs when $\gamma_f(n) \leq 0$. In this case, the dissociation is barrierless and occurs at a critical value of the driving force, i.e., when $\gamma_f = 0$. The *potency* of a nucleation site can be defined by the thickness n (number of crystal planes) of the nucleus that can be produced from the defect by barrierless dissociation. The critical value n^* for nucleation follows from Eq. (1) and the condition $\gamma_f = 0$ as

$$n^* = -\frac{2\gamma_s}{\rho(\Delta G_{ch} + E_{str} + W_f)}. \tag{2}$$

The critical n^* for martensitic nucleation is temperature-dependent through the term ΔG_{ch}. We will show later that it could also be stress-dependent, through the addition of a stress-dependent mechanical driving force ΔG_σ in the denominator of (2). The critical value n^* also depends on the chemical composition of the austenite through the compositional dependence of ΔG_{ch} and W_f.

Let N_v^0 be the total number of nucleation sites of all potencies per unit austenite volume and N_v the number of sites of sufficient potency to nucleate martensite (operational sites) per unit austenite volume. Cohen and Olson [22] derived the cumulative defect-potency distribution dN_v from the Cech and Turnbull small-particle experiments in Fe–30% Ni alloys [23] as

$$dN_v = dN_v^0 e^{-an^*}, \tag{3}$$

where a is a shape factor.

The model developed in this work is based on a modification of the potency distribution of Eq. (3); the modification is based on Kuroda's [24] suggestion that the overall potency distribution is the sum of the stress-modified and strain-modified distributions of nucleation sites: $dN_v = dN_v^\sigma + dN_v^\varepsilon$. This accounts for the effects of stress σ and plastic strain ε on the evolution of the number of operational sites N_v in a uniaxial tension test. The modification of the potency distribution by stress and strain is described in Sections 2.2 and 2.3 respectively, while the overall potency distribution is described in Section 2.4.

2.2. Potency distribution for stress-assisted transformation

Application of a uniaxial stress σ that causes only elastic strains can trigger martensitic nucleation through a mechanical contribution $\Delta G_\sigma(\sigma)$ to the chemical driving force ΔG_{ch}

$$n^*(\sigma) = -\frac{2\gamma_s}{\rho[\Delta G_{ch} + \Delta G_\sigma(\sigma) + E_{str} + W_f]}. \tag{4}$$

The potency distribution of Eq. (3) becomes

$$dN_v^\sigma(\sigma) = dN_v^{\sigma 0} e^{-a_\sigma n^*(\sigma)}, \quad (5)$$

where a_σ is the shape factor in the stress-modified distribution.

If we make the assumption that the variation of ΔG_σ with σ is insignificant, then n^* is constant to first approximation and the last equation can be integrated to yield

$$N_v^\sigma = N_v^{\sigma 0} \exp(-a_\sigma n^*) \quad (6)$$

2.3. Potency distribution for strain-induced transformation

Plastic strain in the austenite phase generates new nucleation sites and the factor dN_v^0 in Eq. (3) depends on plastic strain. Let N be the maximum number of sites per unit austenite volume and N_v^0 the total number of nucleation sites of all potencies per unit austenite volume. In a uniaxial tension test an increment of plastic strain $d\varepsilon$ causes a change $dN_v^{\varepsilon 0}$, which is proportional to the number of available nucleation sites $N - N_v^0$; it is also assumed that $dN_v^{\varepsilon 0}$ is proportional to the value of plastic strain ε raised to a power, say $m-1$, i.e., we write

$$dN_v^{\varepsilon 0} = (N - N_v^{\varepsilon 0})\alpha\varepsilon^{m-1}\, d\varepsilon, \quad (7)$$

where α is a proportionality constant. Then

$$dN_v^\varepsilon = dN_v^{\varepsilon 0}(\varepsilon)\exp[-a_\varepsilon n^*(\sigma)], \quad n^*(\sigma) = -\frac{2\gamma_s}{\rho[\Delta G_{ch} + \Delta G_\sigma(\sigma) + E_{str} + W_f]}, \quad (8)$$

where a_ε is the shape factor in the strain-modified distribution. Eq. (7) can be integrated to yield

$$N_v^{\varepsilon 0}(\varepsilon) = N[1 - \exp(-k\varepsilon^m)], \quad k = \frac{\alpha}{m}, \quad (9)$$

where the initial condition $N_v^{\varepsilon 0}(0) = 0$ has been used.

Again, if we make the assumption that the variation of ΔG_σ with σ been insignificant, then n^* is constant to first approximation and Eq. (8) can be integrated to yield

$$N_v^\varepsilon(\varepsilon) = N_v^{\varepsilon 0}(\varepsilon)\exp(-a_\varepsilon n^*), \quad (10)$$

where $N_v^{\varepsilon 0}(\varepsilon)$ is defined by Eq. (9) above.

2.4. Overall potency distribution and transformation fraction

Let V^a the austenite volume, V^m the martensite volume, and $V = V^a + V^m$ the total volume, so that the volume fraction of martensite is $f = V^m/V$. If N_v changes to $N_v + dN_v$, the martensite volume created per unit austenite volume is $v_p\, dN_v$, where v_p is the average volume of the austenite particles (here we assume that the martensite volume equals the austenite volume; a correction that accounts for volume change is possible). The total change in martensite volume dV^m due to dN_v is

$$dV^m = (v_p\, dN_v)V^a = (V - V^m)v_p\, dN_v. \quad (11)$$

If we divide the last equation by the total volume V, we find that

$$\frac{dV^m}{V} = \left(1 - \frac{V^m}{V}\right)v_p\, dN_v \text{ or } df = (1-f)v_p\, dN_v, \quad (12)$$

which is integrated to yield

$$f(N_v) = 1 - \exp(-v_p N_v) \quad \text{with } N_v = N_v^\sigma + N_v^\varepsilon, \quad (13)$$

where we took into account that f vanishes for $N_v = 0$.

If we now make the assumption that the variation of ΔG_σ with σ is insignificant, then Eqs. (6) and (10) can be used for the evaluation of N_v^σ and N_v^ε; in that case the above expression (13) for the martensite volume fraction f can be written in the following

form:

$$f(\varepsilon) = 1 - \exp[-v_p N_v(\varepsilon)], \quad (14)$$

where

$$N_v(\varepsilon) = N_v^\sigma + N_v^\varepsilon(\varepsilon), \quad (15)$$

$$N_v^\sigma = N_v^{\sigma 0} \exp(-a_\sigma n^*), \quad (16)$$

$$N_v^\varepsilon(\varepsilon) = N_v^{\varepsilon 0}(\varepsilon)\exp(-a_\varepsilon n^*), \quad N_v^{\varepsilon 0}(\varepsilon) = N[1 - \exp(-k\varepsilon^m)]. \quad (17)$$

When the plastic strain ε vanishes, f takes on the stress-assisted portion of the transformation f_{SA}. According to Eq. (14) we have

$$f_{SA} \equiv f(0) = 1 - \exp(-v_p N_v^\sigma). \quad (18)$$

It is interesting to note that the amount of transformation depends on the size of the austenite particles through v_p in (14) and (18). In fact, the volume fraction f increases with the particle size v_p.

3. Fitting the model to available experimental data

3.1. Experimental steels

The result described by Eq. (14) was fitted to available experimental data by Samek et al. [7] and Itami et al. [25]. The chemical composition of the steels used from these works is shown in Table 2.

Steels 1 and 4 are typical CMnSi steels, Steel 2 is a CMnSiAl steel with partial replacement of Si with Al, and Steel 3 is a CMnSiAlP steel with partial replacement of Si with Al and P. In all steels under consideration the TRIP microstructures were obtained by a two-step heat treatment consisting of intercritical annealing followed by holding at the bainitic isothermal transformation temperature. The resulting microstructures in all cases consisted of ferrite, bainite and retained austenite. Steels 1–3 have received identical heat treatment. Steel 4 has three variants corresponding to three holding times (10, 60 and 480 s) at the bainite transformation temperature of 400 °C. These variants are listed as Steel 4/10, Steel 4/60 and Steel 4/480 respectively. The transformation fraction f was determined as a function of plastic strain ε by measuring the saturation magnetization interrupted tensile testing. In Steels 1–3 the measurements were performed for temperatures in the range of 10–100 °C whereas in Steel 4 the measurements were performed at room temperature. Details on retained austenite volume fraction and particle size as well as chemical composition of austenite are given in [1,16].

In order to apply the model to the steels of Table 2, various components entering Eqs. (15)–(17) have to be calculated as described in the following.

3.2. Chemical driving force

The chemical driving force ΔG_{ch} for martensitic transformation of austenite particles is a function of chemical composition (primarily carbon and manganese in the austenite) and temperature. The chemical driving force for martensitic transformation is defined as

$$\Delta G_{ch} = G(bcc) - G(fcc) \quad (19)$$

where $G(bcc)$ and $G(fcc)$ are the free energies of bcc and fcc phases of the same composition. These free energies were calculated with the Thermo-Calc software system by employing the TCFE6 database [26]. The results for Steels 1–3 are given as a function of

Table 2
Chemical composition (mass%) of the steels considered in this study.

Steels	C	Mn	Si	Al	P	Reference
Steel 1	0.24	1.61	1.45	0.03	0.006	[7]
Steel 2	0.25	1.70	0.55	0.69	0.007	[7]
Steel 3	0.19	1.68	0.48	0.84	0.066	[7]
Steel 4	0.14	1.66	1.94	0.025	0.008	[25]

temperature as follows:

$$\text{Steel 1}: \Delta G_{ch}(T) = -5071.56 + 7.12T \ (J/mol) \tag{20}$$

$$\text{Steel 2}: \Delta G_{ch}(T) = -4755.31 + 6.95T \ (J/mol) \tag{21}$$

$$\text{Steel 3}: \Delta G_{ch}(T) = -4470.02 + 6.79T \ (J/mol) \tag{22}$$

where T is the temperature in K.

Regarding chemical stabilization, retained austenite in Steel 1 has the lowest stability whereas the retained austenite in Steel 3 has the highest stability. The retained austenite in Steel 2 possesses an intermediate stability between the other two steels. These observations are in accordance with the carbon content of retained austenite as determined in [7]. For Steel 4 the ΔG_{ch} term was calculated at 20 °C, since the fraction martensite vs strain data were obtained at room temperature. The calculations were carried out for the three variants and the results are -2546, -2341 and -2091 J/mol for the 4/10, 4/60 and 4/480 variants respectively.

3.3. Mechanical driving force

The mechanical driving force contribution ΔG_σ is proportional to the applied stress σ

$$\Delta G_\sigma = \sigma \frac{\partial \Delta G}{\partial \sigma} \tag{23}$$

and is given as a function of the stress-state by Patel and Cohen [27] as

$$\frac{\partial \Delta G}{\partial \sigma} = -0.715 - 0.3206 \frac{\sigma_h}{\overline{\sigma}} \ (J/mol \ MPa), \tag{24}$$

where $\sigma_h = \sigma_{kk}/3$ is the hydrostatic stress and $\overline{\sigma}$ is the von Misses equivalent stress. The ratio $\sigma_h/\overline{\sigma}$ is known as the "triaxiality" of the stress state. In uniaxial tension, $\sigma_h/\overline{\sigma} = 1/3$ and the mechanical driving force contribution from Eq. (24) is -0.822 J/mol MPa. In considering stress effects on the potency distribution of Eq. (3), two limiting cases are considered. First, a fully-biased distribution is considered, which is based on the assumption of Patel and Cohen [27] that the operative nucleation sites have an optimum orientation for maximum interaction with the applied stress. In this case, the ΔG_σ term is given by Eqs. (23) and (24) and is used in Eq. (8) for the calculation of n^*. Second, we consider the opposite extreme of a fully-random distribution, which is based on the assumption by Olson et al. [28] that the nucleation sites are randomly oriented. In this case, ΔG_σ is approximately one third (1/3) of that predicted by the fully-biased distribution. Therefore, the ΔG_σ term is replaced by $\Delta G_\sigma/3$ in Eq. (4), which describes the potency distribution in the stress-assisted transformation regime. The value of stress in Eq. (23) was taken equal to the yield strength of retained austenite. A value of 550 MPa was adopted from the work of Samek et al. [7] for Steels 1–3, while the values 382, 382 and 527 MPa were adopted for steel variants 4/10, 4/60 and 4/480 respectively from the work of Itami et al. [25].

3.4. Frictional work of interfacial motion

The frictional work of interfacial motion during martensitic nucleation W_f is a function of chemical composition of retained austenite. Taking into account the treatment of Labusch [29], where the solution hardening effect is proportional to the 2/3 power of the alloying elements, and adopting the data of Kuroda [24] for Fe–C–Mn alloys, we obtain the following 2/3 power–law expression:

$$W_f = 1.893 \times 10^3 X_{Mn}^{2/3} + 1.310 \times 10^4 X_C^{2/3} \ (J/mol) \tag{25}$$

where X_{Mn} and X_C are the mole fractions of Mn and C in the austenite.

3.5. Shape parameters and other constants

For the Fe–30% Ni small particle experiments of Cech and Turnbull [23], the shape parameter of the potency distribution of Eq. (3) has been evaluated by Olson and Cohen [22] to be $a = 0.866$. For the less stable retained austenite in the low alloy Fe–Mn–C steels considered in this work, the shape parameter for the pre-existing nucleation sites should have a much lower value. The value of $a_\sigma = 0.1$ was used in Eq. (5) for the stress-modified distribution. Based on the assumption that the nucleation sites created by plastic strain are more potent than the pre-existing sites, a lower value of $a_\varepsilon = 0.03$ was adopted for the strain-modified potency distribution in Eq. (8). The values of the remaining parameters were taken from [30,31] as follows: $E_{str} = 500$ J/mol, $\gamma_s = 0.15$ J/m², $\rho = 3 \times 10^{-5}$ mol/m², $k = 46$, and $n = 3.45$. The measurements of austenite particle size by TEM in [7] suggest a mean radius $R = 1$ μm, which corresponds to an average volume of austenite particles of $v_p = (4/3)\pi R^3 = 4.18 \times 10^{-18}$ m³. The values of the various parameters used in this work are summarized in Table 3.

3.6. Fitting parameters

Non-linear curve fitting was performed with fitting parameters: (i) the pre-existing nucleation sites $N_v^{\sigma 0}$ and (ii) the maximum sites that can be produced by plastic deformation N per unit volume. The calculated values of the fitting parameters for all temperatures and steel compositions considered are quite stable and of the order of 1.5–4×10^{17} m⁻³ for $N_v^{\sigma 0}$ and 1.9–5×10^{19} m⁻³ for N. The calculated values of $N_v^{\sigma 0}$ are consistent with that of 2×10^{17} m⁻³ reported in [24] for Cu–Fe alloys and the value of 10^{16} m⁻³ reported in [32] for ceramic systems.

3.7. Effect of austenite composition

The effect of chemical stabilization of retained austenite, arising mainly from carbon partitioning, is shown in Fig. 1, where the volume fraction of martensite f, as predicted by Eq. (14), is plotted against axial plastic strain and compared to experimental data from interrupted tensile testing. Fig. 1a, b and c corresponds to testing temperatures of 10, 20 and 65 °C for Steels 1–3 of Table 2. Fig. 1d corresponds to 20 °C for the three variants of Steel 4 (variants 4/10, 4/60, 4/480). The model predicts well the sigmoidal shape of the strain-induced transformation, i.e., initially the rate of

Table 3
Values of various parameters used in this work.

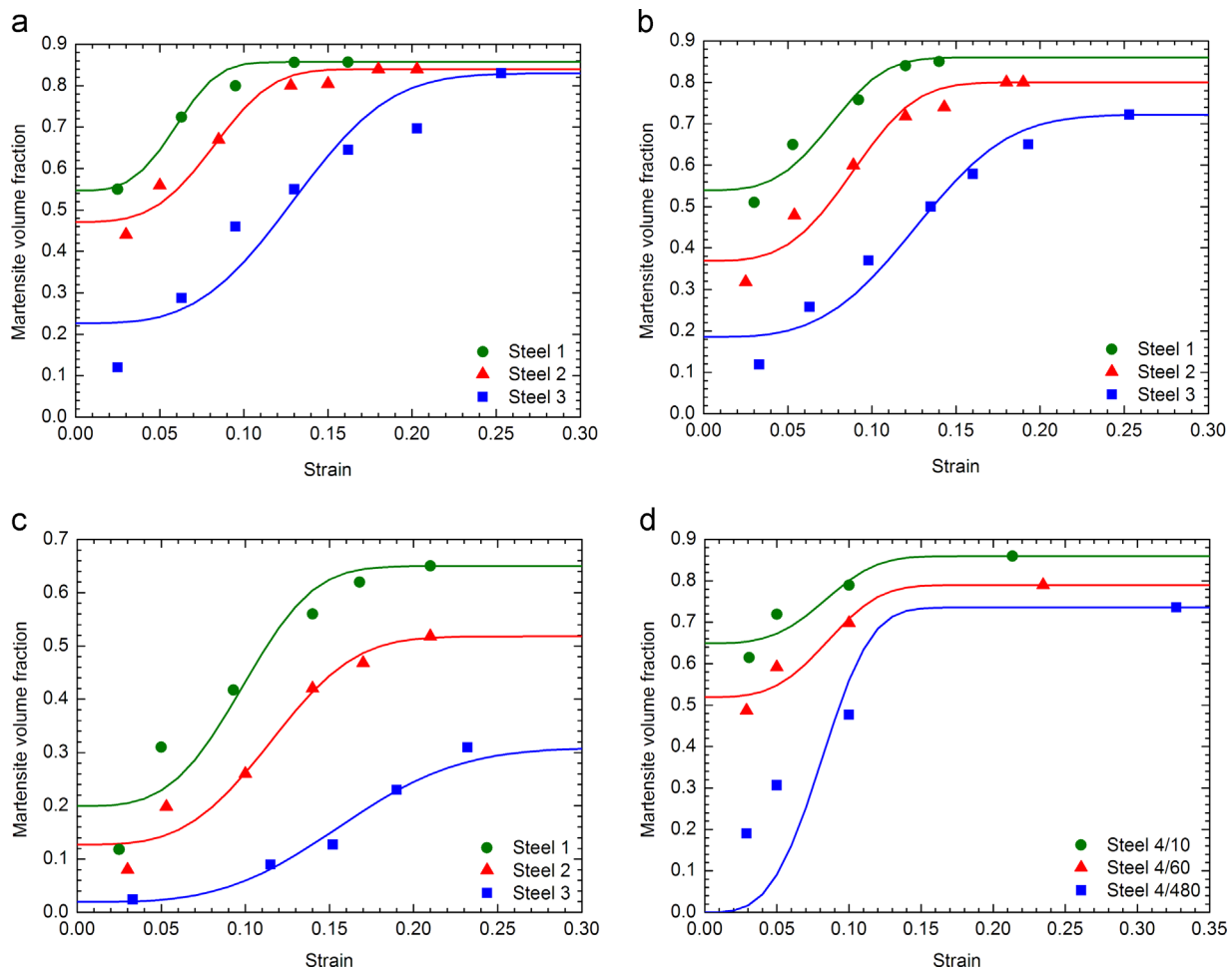| Parameter	Value	Parameter	Value
a_σ	0.1	ρ	3×10^{-5} mol/m²
a_ε	0.03	k	46
E_{str}	500 J/mol	m	3.45
γ_s	0.15 J/m²	v_p	4.18×10^{-18} m³

Fig. 1. Variation of martensite volume fraction f with axial plastic strain ε. Comparison of model and experimental data: (a) 10 °C, (b) 20 °C, (c) 65 °C for Steels 1–3 and (d) 20 °C for Steels 4/10, 4/60, 4/480.

transformation increases with strain, reaches a fairly constant rate $df/d\varepsilon$ and then the rate decreases at higher strains as saturation is approached. Regarding Steels 1–3, the model predicts higher transformation fractions for Steel 1, lower for Steel 3, and intermediate fractions for Steel 2 at the three temperatures and for the strain range considered, reflecting the effect of chemical stabilization of retained austenite, in accordance with the discussion in Section 3.2. The same holds for the three variants of Steel 4 in Fig. 1d, where in Steel 4/10 the retained austenite possesses the lowest stability, Steel 4/480 the highest and Steel 4/60 an intermediate stability, in accordance with the chemical driving force calculations presented in the previous section.

In Fig. 1a–d, the value f at zero plastic strain ($\varepsilon = 0$) is the aforementioned stress-assisted portion of the transformation f_{SA} and agrees well with the experimental data. In the stress-assisted case, the transformation is exclusively triggered by the pre-existing nucleation sites. The value of f_{SA} increases as the chemical stability of retained austenite decreases.

Other important aspects are the constant transformation rate $df/d\varepsilon$ and the saturation level at high strains. The rate $df/d\varepsilon$ and the saturation level follow the chemical stabilization of retained austenite, i.e., $df/d\varepsilon$ increases as the chemical stability of retained austenite decreases. The difference between the saturation levels of Steels 1–3 is high at 65 °C and almost diminishes at 10 °C. It is important to note that, for the temperatures considered, the saturation level does not reach the value of 1 (complete transformation).

3.8. Effect of temperature

The effect of temperature on the kinetics of strain-induced transformation is shown in Fig. 2 for Steels 1–3. The transformation fraction increases with decreasing temperature due to the increase of the chemical driving force ΔG_{ch}. The rate $df/d\varepsilon$ and the saturation level also increase with decreasing temperature due to the temperature dependence of the driving force.

4. Implications of the model

The model presented above predicts the evolution of martensite during strain-induced transformation taking into account the effects of the chemical composition of austenite, temperature, average size of austenite particles and stress triaxiality. In this section the effect of temperature on the stress-assisted portion of the transformation is discussed together with the effects of austenite particle size and stress triaxiality.

4.1. Stress-assisted transformation

It was shown in the previous section that both the transformation fraction and the transformation rate increase with decreasing temperature. The same holds for the stress-assisted portion of transformation f_{SA}, which is plotted against temperature in Fig. 3. It is clear that
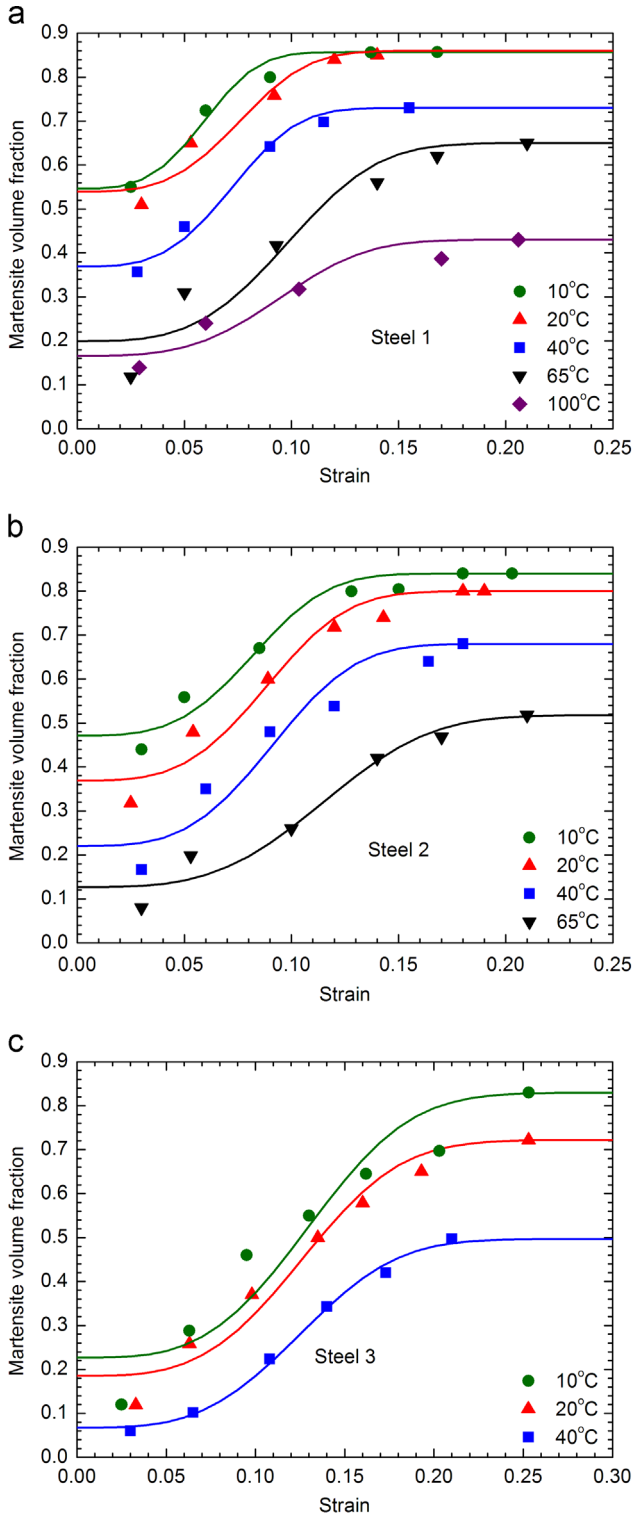
Fig. 2. Variation of martensite volume fraction f with axial plastic strain ε. Comparison of model with experimental data for (a) Steel 1, (b) Steel 2 and (c) Steel 3.
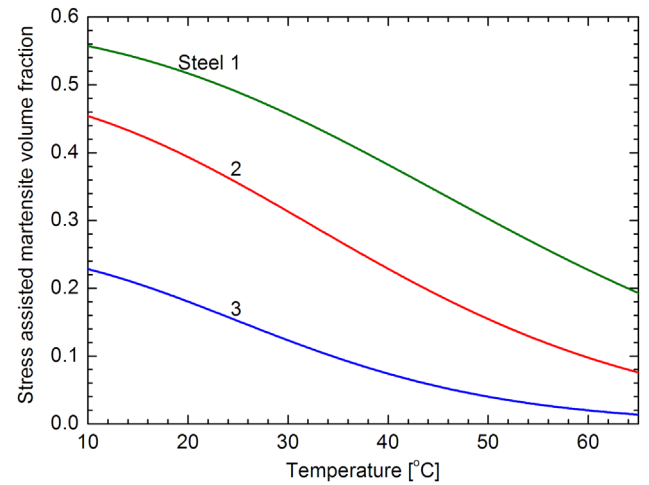

Fig. 3. Volume fraction of martensite formed through stress-assisted transformation (f_{SA}) as a function of testing temperature T for Steels 1–3.
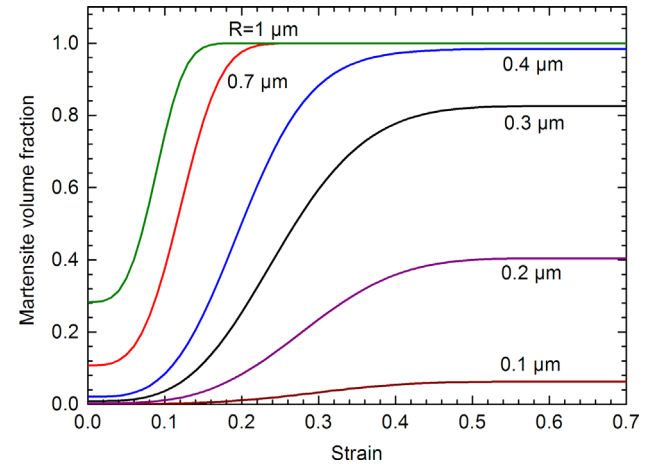

Fig. 4. Effect of particle size on the $f - \varepsilon$ curve for a steel with 0.8 mass% C ($T = 20$ °C). R is the radius of the spherical austenite particles.

the lower the temperature, the higher the contribution of stress-assisted transformation relative to the strain-induced transformation.

4.2. Effect of austenite particle size

In order to investigate the effect of the austenite particle size, the model was applied to an austenite-containing steel for the

following conditions: carbon content of retained austenite 0.8 mass%, tensile testing temperature 20 °C, $N_v^{\sigma 0} = 2 \times 10^{17}$ m^{-3} and $N = 2 \times 10^{19}$ m^{-3}. The yield strength of retained austenite was taken equal to 550 MPa. According to Eq. (14), the particles size affects the transformation through ν_p, the average volume of the austenite particles. The austenite particles are assumed to be spherical with radius R, so that $\nu_p = (4/3)\pi R^3$. The results are shown in Fig. 4 where the transformation fraction f is plotted as a function of plastic strain ε for spherical austenite particles with 0.1–1.0 μm average radius. The stabilizing effect of austenite particle size refinement is evident. For example, at $\varepsilon = 0.2$, while the transformation in the steel containing 1 μm-sized particles has been completed, the transformation for the steel with 0.1 μm-sized austenite particles has barely started. In addition the transformation rate $df/d\varepsilon$ increases with the size of the austenite particles and the transformation is completed ($f = 1$) only for steels containing large particles.

4.3. Effect of stress triaxiality

Stress triaxiality (stress state) influences the transformation kinetics through the interaction with the transformation dilatation. The effect is complex and to a first approximation can be taken into account through the mechanical driving force contribution, as described by Eqs. (23) and (24). In order to investigate the
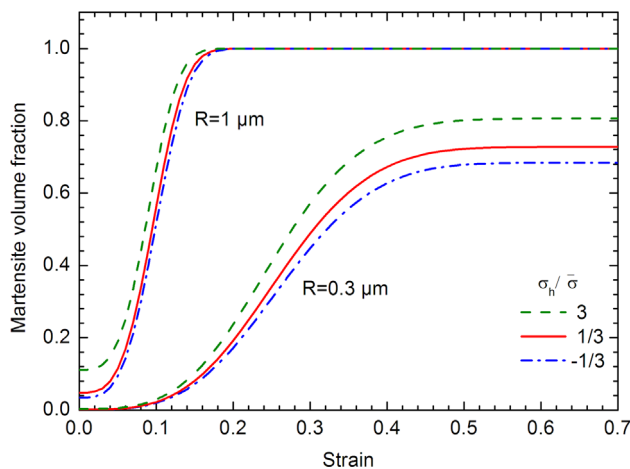
Fig. 5. Effect of stress triaxiality on the $f - \varepsilon$ curve for a steel with 1 mass% C ($T=20\,°C$, $R=1\,\mu m$ and $R=0.3\,\mu m$).

effect of stress triaxiality, the model was applied to a steel containing dispersed austenite of higher carbon content (1 mass %), which reduces the chemical driving force ΔG_{ch}. This leads to an increased relative contribution of the mechanical driving force ΔG_σ to the total driving force and emphasizes the effect of stress triaxiality. The temperature was set to 20 °C and two cases regarding the average austenite particle size were considered: 1 and 0.3 μm radius. The same $N_v^{\sigma 0}$ and N values as in the case of Section 4.2 were adopted. The results are shown in Fig. 5, where the transformation fraction is plotted as a function of plastic strain for three values of the triaxiality factor $\sigma_h/\overline{\sigma}$: $-1/3$ corresponding to uniaxial compression, 1/3 corresponding to uniaxial tension, and 3, which is a relatively high triaxiality factor representing a stress state ahead of a plastically deforming plane-strain mode-I crack tip. Relative to the case of uniaxial tension, uniaxial compression results in a lower transformation fraction, whereas the high-triaxiality crack-tip stress state results in a higher fraction of transformation. The effect of stress triaxiality changes with the average austenite particle size. In the less stable 1 μm particle dispersion, stress triaxiality affects the stress-assisted transformation and the strain-induced transformation at low strains, whereas in the more stable 0.3 μm particle dispersion the stress triaxiality effect is stronger at higher plastic strains. As shown in Fig. 5, the stress triaxiality effect is not as strong as the particle size effect (Fig. 4); however, as stated above, it could become important in austenitic dispersions with high chemical stability.

4.4. Applications of the model

The model can be used for the development of a constitutive model for the mechanical behavior of TRIP steels containing austenite dispersions. Such constitutive models have been developed, e.g., in [33]; however, at present, they are based on kinetic models for the strain-induced transformation which apply to fully-austenitic steels and do not take into account the particle size effect of the austenitic dispersion. The aforementioned constitutive models are three-dimensional and can be used in connection with the finite element method to predict, not only the tensile behavior, but the more complex stress states encountered in forming operations as well. It is also evident that the model presented above could be used for the microstructural design of these steels in order to achieve the desired mechanical behavior.

It is also worthy of note that whereas all traditional mechanical constitutive equations do not have a "length scale", the present model introduces through v_p an intrinsic "material length", which

is the austenite particle size that can be defined as $\ell = v_p^{1/3}$ or $R = (3v_p/4\pi)^{1/3}$.

5. Conclusions

A model that describes the kinetics of the evolution of martensite volume fraction during the strain-induced transformation of dispersed austenite in low-alloy TRIP steels has been developed. The model is based on the modification of the nucleation site potency distribution by the applied stress and plastic strain for the description of the stress-assisted and strain-induced transformation regimes respectively. The model has been fitted to available experimental data regarding the evolution of martensite as a function of plastic strain for several steels containing austenitic dispersions. The model predicts the sigmoidal shape of the transformation fraction with plastic strain and responds well to the effects of temperature and chemical composition of austenite for all steels considered in this work.

Besides chemical composition of retained austenite and temperature, the model takes into account the effects of austenite particle size and stress triaxiality. Austenite particle size refinement has a strong stabilizing influence by retarding the strain-induced transformation kinetics. Stress triaxiality becomes important in stabilized austenite dispersions (either chemically stabilized or by size refinement) by enhancing the kinetics of the strain-induced transformation.

The kinetic model can be used for the development of a constitutive model describing the three-dimensional mechanical behavior of TRIP steels.

References

[1] R. Zhu, S. Li, I. Karaman, R. Arroyave, T. Niendorf, H.J. Maier, Acta Mater. 60 (2012) 3022–3033.
[2] J.H. Ryu, J.I. Kim, H.S. Kim, C.-S. Oh, H.K.D.H. Bhadeshia, D.-W. Suh, Scr. Mater. 68 (2013) 933–936.
[3] C. Garcia-Mateo, F.G. Caballero, J. Mater. Sci. 44 (2009) 4617–4624.
[4] R. Zhu, S. Li, M. Song, I. Karaman, R. Arroyave, Mater. Sci. Eng. A 569 (2013) 137–143.
[5] Z.H. Cai, H. Ding, X. Xue, J. Jiang, Q.B. Xin, R.D.K. Mishra, Scr. Mater. 68 (2013) 865–868.
[6] Y.F. Shen, Y.D. Liu, X. Sun, Y.D. Wang, L. Zuo, R.D.K. Misra, Mater. Sci. Eng. A 583 (2013) 1–10.
[7] L. Samek, E. De Moor, J. Penning, B.C. De Cooman, Metall. Mater. Trans. A 37A (2006) 109–124.
[8] T. Angel, J. Iron Steel Inst. 177 (1954) 165–174.
[9] D.C. Ludwingston, J.A. Berger, J. Iron Steel Inst. 207 (1969) 63–69.
[10] O. Matsumura, Y. Sakuma, H. Takechi, Scr. Metall. 21 (1987) 1301–1306.
[11] J. Burke, Kinetics of Phase Transformations in Metals, Pergamon Press, Oxford, United Kingdom, 1965.
[12] N. Tsuchida, Y. Tomota, Mater. Sci. Eng. A 285 (2000) 345–352.
[13] K. Sugimoto, M. Kobayashi, S. Hashimoto, Metall. Mater. Trans. A 23A (1992) 3085–3091.
[14] G.B. Olson, M. Cohen, Metall. Trans. A 6A (1975) 791–795.
[15] S. Zhang, K.O. Findley, Acta Mater. 61 (2013) 1895–1903.
[16] Q. Zhou, L. Qian, J. Tan, J. Meng, F. Zhang, Mater. Sci. Eng. A 578 (2013) 370–376.
[17] R. Blonde, E. Jimenez-Melero, L. Zhao, N. Schell, E. Bruek, S. van der Zwaag, N.H. van Dijk, Mater. Sci. Eng. A 594 (2014) 125–134.
[18] G.B. Olson, Encyclopedia of Materials: Science and Technology, Elsevier Science Ltd., USA (2001) 2381–2384.
[19] G.B. Olson, M. Cohen, Metall. Trans. A 7A (1976) 1897–1904.
[20] G.B. Olson, M. Cohen, Metall. Trans. A 7A (1976) 1905–1914.
[21] G.B. Olson, M. Cohen, Metall. Trans. A 7A (1976) 1915–1923.

[22] M. Cohen, G.B. Olson, Proceedings of the First JIM International Symposium (JIMIS-1) Kobe, JapanM. Cohen, G.B. Olson, Suppl. Trans. JIM 17 (1976) 93–98.
[23] R.E. Cech, D. Turnbull, Trans. AIME 206 (1956) 124–132.
[24] Y. Kuroda, Kinetics of deformation-induced transformation of dispersed austenite in two alloy systems (S.M. thesis), Massachusetts Institute of Technology, 1987.
[25] A. Itami, M. Takahashi, K. Ushioda, ISIJ Int. 35 (1995) 1121–1127.
[26] J.O. Anderson, T. Helander, L. Hoglund, P. Shi, B. Sundman, Calphad 26 (2002) 273–312.
[27] J.R. Patel, M. Cohen, Acta Metall. 1 (1953) 531–538.
[28] G.B. Olson, K. Tsuzaki, M. Cohen, MRS Proc. 57 (1987) 129–148.
[29] R. Labush, Phys. Status Solidi 41 (1970) 659–669.
[30] G.N. Haidemenopoulos, M. Grujicic, G.B. Olson, M. Cohen, Acta Metall. 37 (1989) 1677–1682.
[31] G.N. Haidemenopoulos, A.N. Vasilakos, Steel Res. 67 (1996) 513–519.
[32] I.-Wei ChenY-H. Chiao, K. Tsuzaki, Acta Mater. 33 (1985) 1847–1859.
[33] I. Papatriantafillou, M. Agoras, N. Aravas, G.N. Haidemenopoulos, Comput. Methods Appl. Mech. Eng. 195 (2006) 5094–5114.